Desalination and Water Treatment
www.deswater.com

doi: 10.1080/19443994.2015.1017010

57 (2016) 7166–7174
April

Taylor & Francis
Taylor & Francis Group

Preparation of modified cellulose acetate membranes using functionalized multi-walled carbon nanotubes for forward osmosis

Haiyang Jin, Yangbo Huang, Xin Wang, Ping Yu*, Yunbai Luo

College of Chemistry and Molecular Sciences, Wuhan University, Hubei, Wuhan 430072, P.R. China, Tel. +86 27 68752511; email: haiyang@whu.edu.cn (H. Jin), Tel. +86 13 667151729; email: bobo180899@whu.edu.cn (Y. Huang), Tel. +86 13 659834359; email: wangx404@pku.edu.cn (X. Wang), Tel. +86 13 264716120; email: yuping@whu.edu.cn (P. Yu), Tel. +86 13 807148090; email: ybai@whu.edu.cn (Y. Luo)

Received 9 October 2014; Accepted 1 February 2015

ABSTRACT

Novel modified cellulose acetate (CA) membranes using functionalized multi-walled carbon nanotubes (MWCNTs) were synthesized by phase inversion via immersion precipitation technique. Carboxylated functionalized MWCNTs (F-MWCNTs) were used as additives into the casting solution of CA, 1, 4-dioxane, acetone, lactic acid, and methanol to enhance the forward osmosis (FO) membranes performance. Different contents of F-MWCNTs (0.01, 0.05, and 0.1 wt.%) were added into the casting solution. The novel synthesized CA/F-MWCNTs membranes were characterized by various methods in terms of membranes structure and surface properties, as well as FO performance, and then compared with traditional CA membrane and commercial FO membrane. The surface hydrophilicity, porosity, and tensile strength of CA/F-MWCNTs membranes were improved with the increment of the content of F-MWCNTs in the casting solution. The morphological studies showed that the addition of F-MWCNTs significantly changed the surface properties of the modified CA membranes. The FO performance was evaluated using purified water as feed solution and 1 M NaCl solution as draw solution. The CA/F-MWCNTs membranes showed higher water permeability and salt rejection in the range of 0.01–0.1 wt.% F-MWCNTs content than CA membrane and the commercial FO membrane. These encouraging results suggested that CA/F-MWCNTs membranes showed superior potential to be further developed for FO applications.

Keywords: Carboxylated functionalized MWCNTs; Modified CA membrane; Forward osmosis

1. Introduction

Forward osmosis (FO) is the transportation of water across a selectively permeable membrane from a region of higher water chemical potential to a region of lower water chemical potential. It is driven by a difference in solute concentrations across the membrane that allows passage of water, but rejects most solute molecules or ions. Due to its inherent advantages, such as low energy expenditure [1], low membrane fouling [2], and high water recovery [3], FO process was extensively studied by scientists in various disciplines of science and engineering [4,5]. Now, its applications have showed potential values in seawater desalination [1,4], wastewater treatment [2,6], food

*Corresponding author.

and pharmaceuticals processing [7], controlling drug release [8], electrical power generation [9,10], etc.

However, there are some problems which limit the use of FO, such as flux decline, because of internal concentration polarization, lack of proper draw solute, and effective recovery. Recent works have focused on reducing internal concentration polarization and seeking optimal draw solute. The internal concentration polarization which occurs within the support layer is the main factor that causes the decline of water flux [11,12]. The influence of internal concentration polarization on FO water flux has been investigated by employing different modeling techniques and the solution–diffusion theory [5]. A variety of draw solutes/solutions, include magnetic and/or hydrophilic nanoparticles and organic compounds [13,14], have been investigated in FO process.

In the early study, reverse osmosis membranes were tested for FO process. But they showed low water flux due to the internal concentration polarization caused by the porous support layer. Hence, a perfect FO membrane should consist of a single active layer without any support layer [15,16]. However, the following reduction in mechanical strength may limit its applicability. Chung's group developed flat-sheet cellulose acetate (CA)-based membranes comprised double- skinned layers that were able to eliminate internal concentration polarization [17,18]. However, the membranes showed low water flux due to the additional resistance to water transport. Thi Phuong Nga Nguyen et al. prepared CTA/CA FO membranes to enhance water flux [19], but relatively high reverse solute flux (RSF) limits the application of the membranes. It is necessary to prepare FO membranes with high water flux and salt rejection at present.

Carbon nanotube (CNT)-based membrane is an emerging technology in membrane development [20]. It has been studied, adding CNTs to polymeric membranes can enhance the membrane properties like water flux, permeability, rejection, and tensile strength [21,22]. The applicability of the suitability of the CNT membranes for seawater desalination was also explored [23,24]. The major problem of using CNTs is their low hydrophilicity and insolubility in the solvent. Hence, in order to improve their dispersion capability and performance, the surface modifications and functionalization of CNTs are carried out [25,26]. Introduction of hydrophilic functional groups is the most common method.

In this research, functionalized MWCNTs (F-MWCNTs) containing carboxylate groups are added into the casting solution of CA, 1, 4-dioxane, acetone, lactic acid, and methanol to prepare the new CA/F-MWCNTs membranes for FO application. Membranes are prepared by phase inversion via immersion precipitation technique. Subsequently, the new CA/F-MWCNTs membranes are characterized in different ways and compared with traditional CA membrane and a kind of commercial FO membrane. The influences of the content of F-MWCNTs on the membrane performance are also reported.

2. Material and methods

2.1. Materials

CA (54.5–56.0 wt.%acetyl) as the main membrane material and 1, 4-dioxane (≥99.5% purity), acetone (≥99% purity), lactic acid (≥99% purity), and methanol (≥99.8% purity) as the solvent were used for preparing the casting solution. Sodium chloride (NaCl, 99% purity) and deionized water were used for membrane performance testing. Disodium carbonate (Na_2CO_3, 99% purity) was used as an effluent for ion chromatography (ICS-900, Dionex, CA, USA). All the reagents mentioned above were purchased from Sinopharm Chemical Reagent Co., Ltd. The nonwoven fabrics as membrane substrates polymer were obtained from Shanghai Tianlue Advanced Textile Co., Ltd. MWCNTs (OD × ID × L: 5 nm × 1.3–2 nm × 50 μm) from Sigma-Aldrich were used for modifying. The prepared membranes were tested against the commercial membranes (Hydration Technology Innovations, HTI): a cartridge membrane made of cellulose triacetate with an embedded polyester screen mesh (CTA-W).

2.2. Functionalization of MWCNTs

MWCNTs were first dealt with a mixed acid solution containing sulfuric acid (H_2SO_4) and nitric acid (HNO_3). In 150 mL H_2SO_4/HNO_3 mixture (3:1 by volume ratio), 100 mg of pristine MWCNTs was added. This solution was ultrasonic vibrated for 2 h and then refluxed under magnetic stirring at 60˚C for 6 h. The carboxylated MWCNTs were filtered with a 0.2 μm CA microfiltration membrane, washed with distilled water until pH increased to natural. The carboxylated MWCNTs were then dried in a vacuum drying oven at 60˚C for 4 h before further treatment.

The reaction scheme of MWCNT functionalization and dispersion in water is shown in Fig. 1.

2.3. Preparation of flat-sheet CA/F-MWCNTs blend membranes

Flat-sheet membranes were prepared by phase inversion via immersion precipitation technique. The

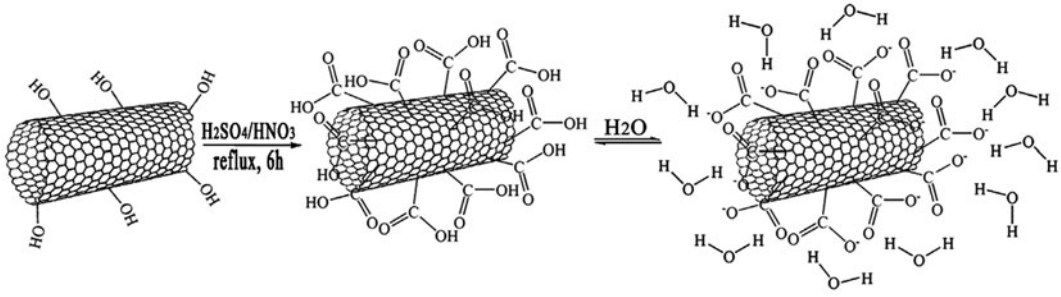

Fig. 1. Reaction scheme of MWCNT functionalization and dispersion in water.

casting solution contained CA polymers dissolved in 1, 4-dioxane and acetone with additives of lactic acid and methanol. The solution was kept in a round flask sealed with a glass stopper to prevent evaporation of the solvents. The solution was homogenized by using a mechanical stirrer (JJ, Yitong Electron Co., Ltd, China). The nonwoven fabric (200 mm × 200 mm pore) was used as a support layer attached to a glass plate by sticky tape. The casting solution was then cast on to this substrate by using an 100 mm thick casting knife in a constant temperature (set up at 25˚C) and humidity (70% relative humidity) room. After evaporation of the solvent for 30 s, the casting film together with the glass plate was immersed in a coagulation bath of 1 ± 0.3˚C deionized water. The resulting CA membrane was then stripped off the glass plate and kept in a bath of deionized water at room temperature (25˚C), which was changed every 4 h for 24 h to wash out the solvents. Then the CA membrane was stored in deionized water for performance testing.

The casting solution was composed of 13.4 wt.% CA, 53.2 wt.% 1, 4-dioxane, 18.4 wt.% acetone, 6.8 wt.% lactic acid, and 8.2 wt.% methanol. The F-MWCNTs were added into the solution in different contents (0.01, 0.05, and 0.1 wt.%) and were dispersed by stirring for 8 h at room temperature. The resultant solution was prepared for phase inversion after eliminating air bladder by ultrasonic vibration. These synthesized CA/F-MWCNTs FO membranes are denoted as CAN 0.01, CAN 0.05, and CAN 0.1 assigned to their nanotubes contents.

2.4. Characterization of membrane structure and surface properties

Scanning electron microscopy (SEM) was used to acquire the cross section and top surface imaging of membranes to determine the morphological properties. The SEM analysis was FEI Quanta 200 from Holland and operated at 15 KV. Every membrane sample was dried under vacuum for 24 h to dehydrate it. Membranes were fractured in liquid nitrogen to clearly scan the cross-section image. The membranes were coated with a gold layer for observation by a sputter coater.

Attenuated total reflectance spectroscopy (ATRFTIR) was used to analyze the chemical changes of the membranes in this study. Nicolet AVATAR 360 FTIR Spectrophotometer together with an ATR accessory (ZnSe crystal) was used to collect the spectra. The incidence angle was 45° and each spectrum was recorded using 32 scans at a resolution of 4 cm^{-1} in the region between 400 and 4,000 cm^{-1}. OMNIC 8.2 software was used to record the spectra, correct their baselines, normalize the spectra, and find the peaks.

Contact angle measurements were conducted by dynamic contact angle instrument (DSA100, KRŰSS GmbH, Hamburg, Germany). Contact angle indicates the hydrophilicity and the smaller angle shows the better hydrophilicity. Every membrane sample was dried under vacuum for 24 h before measurement. Two replicates were used, and five drops per replicate were measured.

Membranes porosity (ε) was calculated from the equations below [27]:

$$\varepsilon = \frac{(m_{\text{wet}} - m_{\text{dry}})/\rho_w}{(m_{\text{wet}} - m_{\text{dry}})/\rho_w + (m_{\text{dry}}/\rho_p)} \times 100 \quad (1)$$

where m_{wet} and m_{dry} are the mass of the hydrated and dried samples, ρ_w and ρ_p are the density of water and polymers at a dried state, respectively. The relative density of the CA polymers used is 1.31 g/cm^3 according to the reagent instructions.

Mechanical properties (e.g. tensile strength) of the synthesized CA membranes and CA/F-MWCNTS membranes were measured using a universal tensile testing machine (AGS-J, Shimazu, Japan). Every membrane sample was dried under vacuum for 24 h before

measurement. The elongation velocity was 2 mm/min with an initial gauge length of 15 mm.

2.5. Performance testing

The prepared membranes were tested in FO mode (Fig. 2) using a test cell with 30.25 cm^2 effective area (width, 6.5 cm; length, 6.5 cm). Either feed solution or draw solution was kept in a 2 L tank. Both solutions were circulated at a rate of 15 L/h in a closed loop by using two diaphragm pumps (PLD-2203, China). The draw solution was placed on a weighing balance and the feed solution was placed on a platform at the same height to eliminate any gravitational effects.

Feed solution was purified water from a Milli-Q system(18 MΩcm) and draw solution was 1 M sodium chloride (NaCl). The volume of both solutions was 1 L. Membrane performances were assessed over 1 h by measuring permeated water flux (J_w) and reverse salt flux (J_s). Data were calculated after running of the system for 5 min to stabilize water flux. The permeate water flux was measured from the change in the weight of the draw solution due to the water permeated over the membrane during the 1 h FO testing as follows:

$$J_w = \frac{\Delta\text{weight}}{\text{water density} \times \text{effective membrane area} \times \Delta\text{time}} \left(l/m^2 \cdot h \text{ or LMH}\right) \quad (2)$$

RSF was determined by ion chromatography which analyzed the concentrations of chloride ions in both solutions during the 1 h FO testing. Before and after1 h testing, 1 mL samples of each solution were collected. RSF was defined as the number of mole of NaCl diffusing from the draw solution to the feed solution per unit time per unit membrane area. The equations were as follows:

$$J_{s-\text{NaCl}} = \frac{\text{mole of NaCl}}{\text{effective membrane area} \times \Delta\text{time}} \quad (\text{moleNaCl}/m^2 \cdot h) \quad (3)$$

The membrane performances were tested in both AL-DS (active layer facing draw solution) and AL-FS (active layer facing feed solution) orientations and compared against commercial FO membranes under similar conditions. All the tests were conducted at 25℃.

3. Result and discussion

3.1. FO membrane morphologies

The cross-section morphology of CA and CA/F-MWCNTs membranes are shown in Fig. 3. Fig. 3(a)–(d) shows that the asymmetric structure of the membranes is not changed by the existence of F-MWCNTs. All the membranes showed the asymmetric structure of compact cortical layer and porous support layer. Furthermore, the finger-like pores increase with the increment of the content of F-MWCNTs. Fig. 3(e)–(h) are the corresponding amplified images of the finger-like structure in Fig. 3(a)–(d) and show that the large pore appears gradually on the surface of the support layer and increases with the increment of the content of F-MWCNTs. The reason for the above changes of the membrane structure is that the existence of F-MWCNTs delays the process of the phase separation during the preparation of membranes, which plays an effect on the membrane structure. These changes lower the resistance during water permeating through the membrane and promote the FO process.

Fig. 4 presents the surface SEM images of CA and CAN 0.1 membranes. It shows that some crosslink structures appear on the surface of CA/F-MWCNTs membranes. The formation of crosslink structures is caused by the reaction between the carboxyl groups of

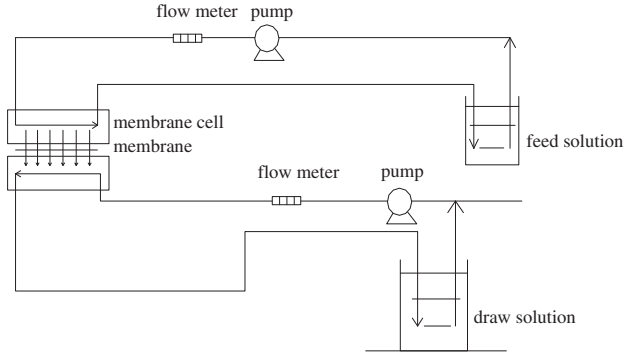

Fig. 2. Laboratory-scale forward osmosis testing.

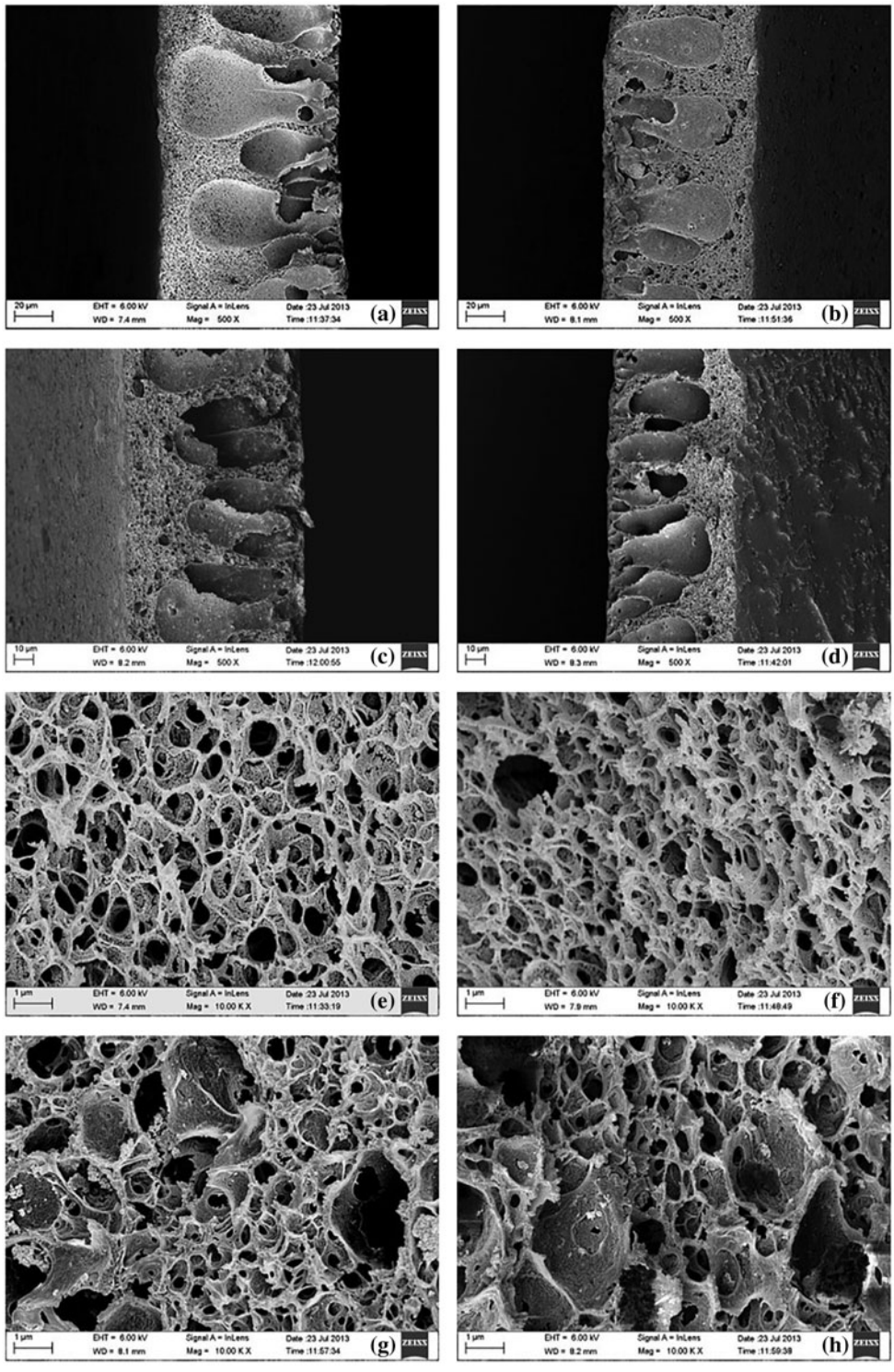

Fig. 3. SEM cross-sectional micrographs of CA and CAN FO membranes with different F-MWCNTs contents: (a) CA, (b) CAN 0.01, (c) CAN 0.05, and (d) CAN 0.1 and amplified SEM cross-sectional micrographs of the spongy structure of CA and CAN FO membranes with different F-MWCNTs contents: (e) CA, (f) CAN 0.01, (g) CAN 0.05, and (h) CAN 0.1.

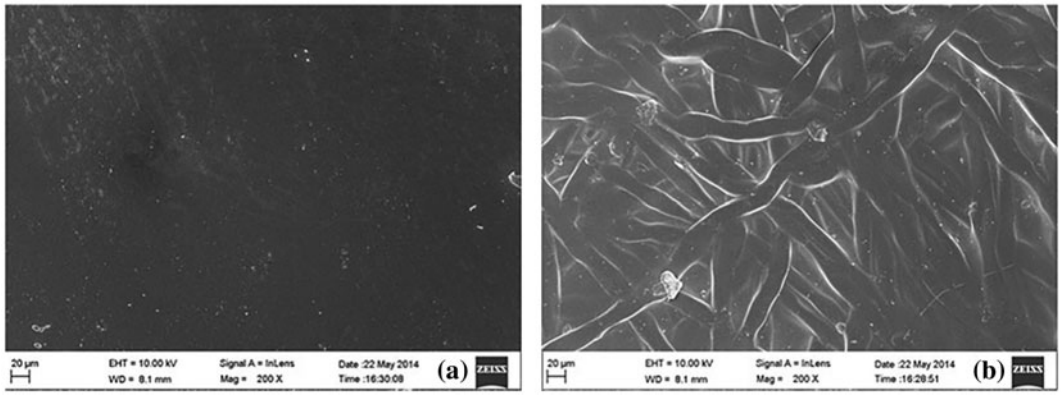

Fig. 4. SEM micrographs displaying the top surfaces of CA and CAN FO membranes: (a) CA and (b) CAN 0.1.

F-MWCNTs and hydroxyl groups of CA polymer. These crosslink structures make the membrane structure more compact. In addition, it is obvious that the surface roughness of the membrane increases due to the existence of crosslink structures.

Table 1 indicated the surface contact angles, porosity, and tensile strength of CA and CA/F-MWCNTs membranes. The contact angle values of membranes declined with the increment of F-MWCNTs content. These results suggested that the incorporation of F-MWCNT developed nanochannels on the surfaces and allowed water droplets expanding on it easily [28]. In addition, the F-MWCNTs increased the hydrophilicity of membranes due to its hydrophilic carboxyl group (−COOH). Furthermore, the improvement of the surface roughness can effect on the increase of hydrophilic. Therefore, a more hydrophilic surface for CA membrane is produced by adding F-MWCNTs in the casting solution. CA/F-MWCNTs membranes have higher porosity than CA membrane because of the increment of the finger-like pores and large pores. However, further increase in F-MWCNTs content showed lower porosity, which might be attributed to the defect of CNTs agglomeration in the phase inversion process. The tensile strength of membranes increased with the increment of F-MWCNTs content due to the crosslink reaction between F-MWCNTs and CA polymer. The properties of the commercial FO membrane (CTA-W) were also pointed in Table 1 and it could be noted that the synthesized membranes had better structure performance for FO process.

3.2. FTIR spectra of pristine MWCNTs, F-MWCNTs, CA, and CA/F-MWCNTs membranes

FTIR spectra of pristine F-MWCNTs containing carboxylic is shown in Fig. 5. Fig. 5(a) shows the FTIR spectrum of unmodified CNTs. The appearance of peaks at 1,640 cm^{-1} is attributed to C=C bond of carbon structure of CNTs. The peak at 3,445 cm^{-1} is attributed to the presence of hydroxyl (−OH) group on the unmodified MWCNTs as shown in Fig. 1, which is resulted from purification of the raw material during oxidation or atmospheric moisture present on the MWCNTs. The FTIR spectrum of carboxylated MWCNTs is presented in Fig. 5(b). Different to Fig. 5(a), the additional peak at 1,710 cm^{-1} is attributed to the carbonyl (C=O) stretching vibration of the carboxylic acid group.

Fig. 6 presents the ATR–FTIR of the CA and CA/F-MWCNTs membranes with different F-MWCNTs contents (0.01, 0.05, and 0.1 wt.%). The appearance of peaks at 1,750 cm^{-1} corresponds to the carbonyl (C=O) of the membrane. The appearance of peaks at 1,040

Table 1
Contact angle, porosity, and mechanical strength of CA and CAN FO membranes

Membranes	Contact angle (°)	Porosity (%)	Tensile strength (MPa)
CA	59.6 ± 0.66	57.18	56.92
CAN 0.01	54.6 ± 0.76	67.87	62.45
CAN 0.05	52.8 ± 0.83	74.15	67.57
CAN 0.1	47.6 ± 0.34	67.18	71.56
CTA-W	71 ± 2	46±1	58

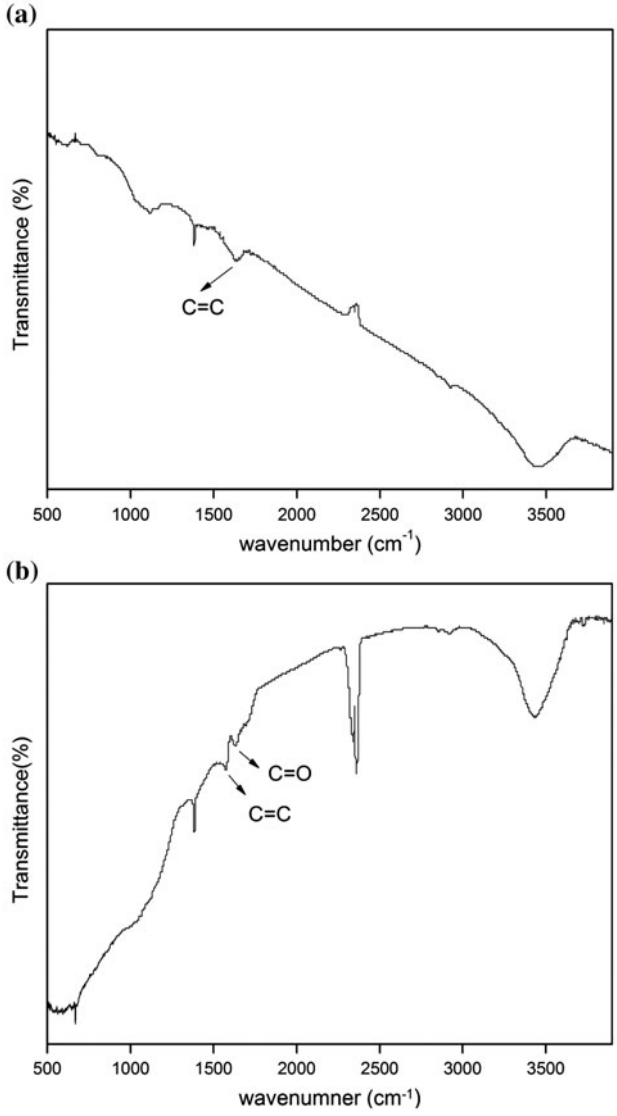

Fig. 5. FTIR spectra of (a) pristine MWCNTs and (b) F-MWCNTs containing carboxyl.

and 1,228 cm^{-1} is assigned to the ether group (C–O–C) of the membrane. The intensity of the peak of the carbonyl increase with the increment of the content of F-MWCTNs due to the increment of C=O group. Meanwhile, the intensity of the two peaks of the ether group also increase with the increment of the content of F-MWCTNs, which might be corresponding to the increment of C–O–C group because of the reaction between F-MWCNTs and CA polymer. The above analyses of the spectra indicate that the carboxylate functional groups are formed on the surface of MWCNTs and there is a linkage between F-MWCNTs and CA polymer.

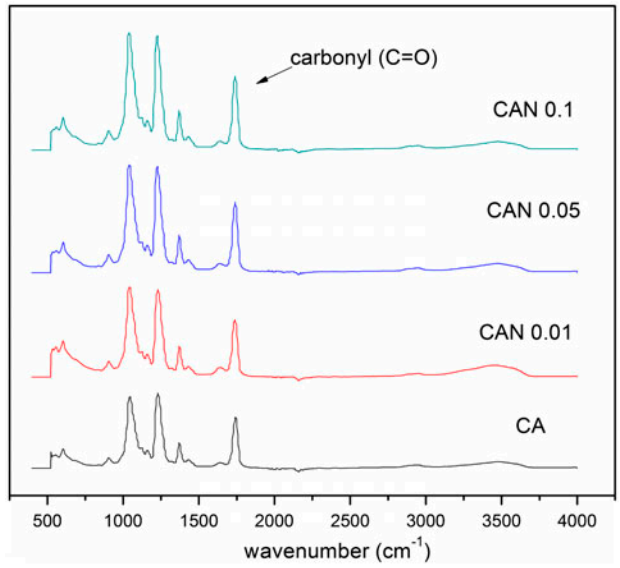

Fig. 6. ATR–FTIR spectra of CA and CAN FO membranes.

3.3. Determination of FO performance

The FO performances of CA and CA/F-MWCNTs membranes including water flux and reverse salt flux are shown in Fig. 7 and the detailed data are listed in Table 2. It should be noted that the synthesized CA/F-MWCNTs FO membranes exhibited high water flux and low reverse salt flux than CA membranes in both AL-DS and AL-FS orientations. In addition, AL-DS represents the higher water flux but also high reverse salt flux comparing to AL-FS orientation. The range of water fluxes changed from 7.5–18.1 L/m^2 h in AL-FS to 9.1–27.1 L/m^2 h in AL-DS due to the more severe ICP in the AL-FS configuration than the AL-DS situation [29]. Comparing the FO water flux of CA and CA/F-MWCNTs FO membranes, it should be noted that water flux increased with the increment of the F-MWCNTs contents. The water flux was improved from 9.1 to 27.1 L/m^2 h in AL-DS when the content of the F-MWCNTs increased from 0 to 0.1 wt.%. The improvement in water flux of CA/F-MWCNTs membranes could be attributed to the existence of F-MWCNTs that form nanochannels in the top surface of the membranes. Both inner cores of nanotubes (internal nanochannels) and the interfacial gap between F-MWCNTs and CA polymer at the interface of CA layer (external nanochannels) create further passage for solvent transfer. The latter plays a dominant role since the internal nanochannels are too thin to extract water without applying pressure (FO mode). Moreover, the external nanochannels create direct and appropriate path in comparison with the inner cores

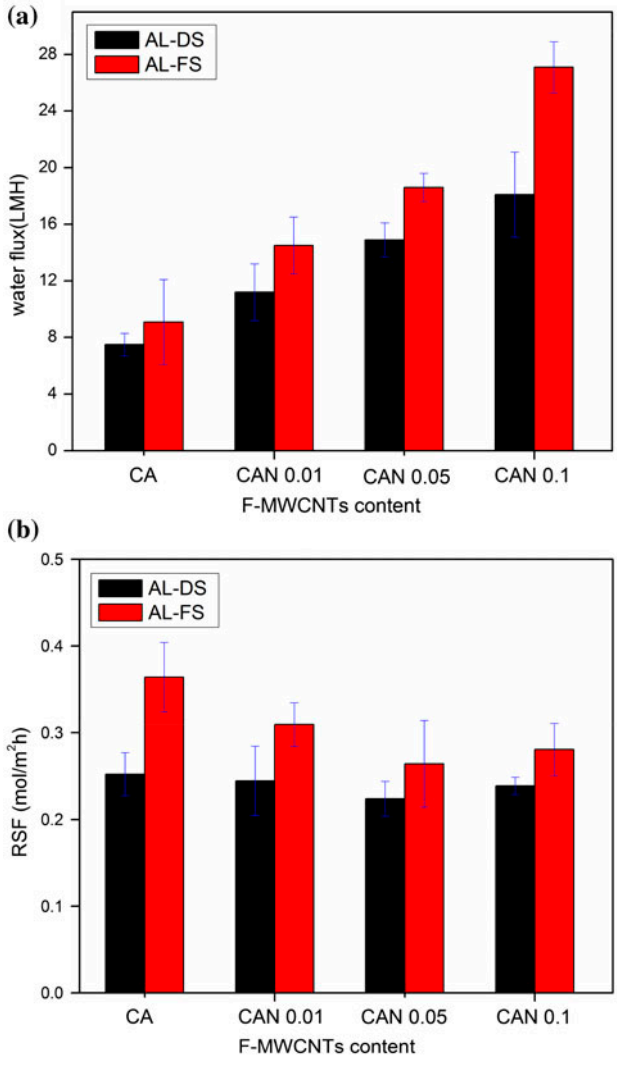

Fig. 7. FO water flux and reverse salt flux of synthesized FO membranes: (a) water flux and (b) reverse salt flux.

Table 2
Performances of CA, CAN, and CTA-W membranes in FO process. DS was 1 M NaCl; FS was purified water at 25°C

Membranes	Water flux J_w (LMH)		Reverse salt flux J_s-NaCl (mole NaCl/m^2 h)	
	AL-DS	AL-FS	AL-DS	AL-FS
CA	7.5	9.1	0.2521	0.3641
CAN 0.01	11.2	14.5	0.2445	0.3094
CAN 0.05	14.9	18.6	0.2239	0.2641
CAN 0.1	18.1	27.1	0.2387	0.2807
CTA-W	8.3	11.3	0.2462	0.3218

[28]. In addition, the presence of F-MWCNTs increases the surface hydrophilicity and roughness of FO membranes, which causes to improve the water permeation through CA/F-MWCNTs FO membranes. The above findings are in agreement with high water permeability of CA/F-MWCNTs membranes. CA/F-MWCNTs membranes also showed low reverse salt flux since the improvement in surface hydrophilicity promotes the membrane adsorbing water preferably, which decrease reverse salt flux. Besides, the F-MWCNTs as a weak acid ionize partly in water and make the membrane surface have some negatively charged carboxylate ions as shown in Fig. 1. It makes the membrane electrostatic to attract water molecules and repel salt anions which decreases reverse salt flux. It should be noted that the increment of F-MWCNTs content led to the decrement of reverse salt flux in all FO membranes except CAN 0.1, which might be attributed to the defect of F-MWCNTs agglomeration in the phase inversion process. According to the solution–diffusion theory, the reverse salt flux is proportional to the salt rejection coefficient R [4]. Therefore, the lower reverse salt flux might be assigned to the higher salt rejection [30]. As the suitable FO membranes should have the high water flux and low reverse salt flux, it revealed that the excessive addition of F-MWCNTs may not be beneficial for FO applications. The performance of the commercial FO membrane (CTA-W) is also listed in Table 2 and it is worthwhile to note that the synthesized CA/F-MWCNTs FO membranes exhibited superior performance. In summary, all of the above results and discussion demonstrate that the CA/F-MWCNTs FO membranes exhibited satisfactory water permeability and salt rejection.

4. Conclusions

Novel CA/F-MWCNTs FO membranes were synthesized through adding carboxylated F-MWCNTs into CA casting solution and compared with CA FO membrane and the commercial FO membrane (CTA-W). CA and CA/F-MWCNTs membranes were prepared by phase inversion via immersion precipitation technique. The incorporation of the F-MWCNTs did not change the asymmetric structure of CA membrane but made the finger-like structure more compact. The surface hydrophilicity, porosity, and tensile strength increased with the increment of F-MWCNTs content in the casting solution. The synthesized CA/F-MWCNTs FO membranes exhibited superior performance than CA and commercial FO membranes. The water flux (in both AL-FS and AL-DS modes) and salt rejection were simultaneously improved in the CA/F-MWCNTs membranes.

However, further addition of F-MWCNTs might affect the immersion precipitation process and decrease the selectivity of the membranes. Finally, it can be concluded that CA/F-MWCNTs membranes have superior potential for FO application as a result of their enhanced structural and separation properties.

Acknowledgments

This work was supported by the National Science and Technology Support Program (2012BAC02B03).

References

[1] R.L. McGinnis, M. Elimelech, Energy requirements of ammonia–carbon dioxide forward osmosis desalination, Desalination 207 (2007) 370–382.
[2] A. Achilli, T.Y. Cath, E.A. Marchand, A.E. Childress, The forward osmosis membrane bioreactor: A low fouling alternative to MBR processes, Desalination 239 (2009) 10–21.
[3] C.R. Martinetti, A.E. Childress, T.Y. Cath, High recovery of concentrated RO brines using forward osmosis and membrane distillation, J. Membr. Sci. 331 (2009) 31–39.
[4] T.Y. Cath, A.E. Childress, M. Elimelech, Forward osmosis: Principles, applications, and recent developments, J. Membr. Sci. 281 (2006) 70–87.
[5] S. Zhao, L. Zou, C.Y. Tang, D. Mulcahy, Recent developments in forward osmosis: Opportunities and challenges, J. Membr. Sci. 396 (2012) 1–21.
[6] E.R. Cornelissen, D. Harmsen, K.F. de Korte, C.J. Ruiken, J.J. Qin, H. Oo, L.P. Wessels, Membrane fouling and process performance of forward osmosis membranes on activated sludge, J. Membr. Sci. 319 (2008) 158–168.
[7] E.M. Garcia-Castello, J.R. McCutcheon, M. Elimelech, Performance evaluation of sucrose concentration using forward osmosis, J. Membr. Sci. 338 (2009) 61–66.
[8] Y.K. Lin, H.O. Ho, Investigations on the drug releasing mechanism from an asymmetric membrane-coated capsule with an in situ formed delivery orifice, J. Controlled Release 89 (2003) 57–69.
[9] R.L. McGinnis, M. Elimelech, Global challenges in energy and water supply: The promise of engineered osmosis, Environ. Sci. Technol. 42 (2008) 8625–8629.
[10] A. Achilli, T.Y. Cath, A.E. Childress, Power generation with pressure retarded osmosis: An experimental and theoretical investigation, J. Membr. Sci. 343 (2009) 42–52.
[11] G.D. Mehta, S. Loeb, Internal polarization in the porous substructure of a semipermeable membrane under pressure-retarded osmosis, J. Membr. Sci. 4 (1978) 261–265.
[12] J.R. McCutcheon, M. Elimelech, Influence of concentrative and dilutive internal concentration polarization on flux behavior in forward osmosis, J. Membr. Sci. 284(1–2) (2006) 237–247.
[13] T.W. Kim, Y. Kim, C. Yun, H. Jang, W. Kim, S. Park, Systematic approach for draw solute selection and optimal system design for forward osmosis desalination, Desalination 284 (2012) 253–260.
[14] S. Adham, J. Oppenheimer, L. Liu, M. Kumar, Dewatering reverse osmosis concentrate from water reuse applications using forward osmosis, Water Reuse Found. Res. Rep. 2007.
[15] J.R. McCutcheon, R.L. McGinnis, M. Elimelech, A novel ammonia–carbon dioxide forward (direct) osmosis desalination process, Desalination 174 (2005) 1–11.
[16] J.C. Su, T.S. Chung, Sublayer structure and reflection coefficient and their effects on concentration polarization and membrane performance in FO processes, J. Membr. Sci. 376 (2011) 214–224.
[17] K.Y. Wang, R.C. Ong, T.S. Chung, Double-skinned forward osmosis membranes for reducing internal concentration polarization within the porous sublayer, Ind. Eng. Chem. Res. 49 (2010) 4824–4831.
[18] S. Zhang, K.Y. Wang, T.S. Chung, H. Chen, Y.C. Jean, G. Amy, Well-constructed cellulose acetate membranes for forward osmosis: Minimized internal concentration polarization with an ultra-thin selective layer, J. Membr. Sci. 360 (2010) 522–535.
[19] T. Nguyen, E. Yun, I. Kim, Y. Kwon, Preparation of cellulose triacetate/cellulose acetate (CTA/CA)-based membranes for forward osmosis, J. Membr. Sci. 433 (2013) 49–59.
[20] K.E. Lange, Get the Salt Out, National Geographic, 2010. Available from: <http://ngm.nationalgeographic.com/big-idea/09/desalination>.
[21] S. Kulprathipanja, Mixed matrix membrane development, Ann. N.Y. Acad. Sci. 984 (2003) 361–369.
[22] E.S. Kim, G. Hwang, M.G. El-Din, Y. Liu, Development of nanosilver and multi-walled carbon nanotubes thin-film nanocomposite membrane for enhanced water treatment, J. Membr. Sci. 394–395 (2011) 37–48.
[23] L. Dumee, J. Lee, K. Sears, B. Tardy, M. Duke, S. Gray, Fabrication of thin film composite polyamide carbon nanotube supported membranes for enhanced performance in osmotically driven desalination systems, J. Membr. Sci. 427 (2012) 422–430.
[24] L. Hai-Lan, J. Yu-Xiang, H. Yang-Dong, Molecular dynamics simulation of the desalination of sea water by a forward osmosis membrane containing charged carbon nanotubes, Acta Phys. Chim. Sin. 28 (2012) 573–577.
[25] C.S. Chen, X.H. Chen, L.S. Xu, Z. Yang, W.H. Li, Modification of multi-walled carbon nanotubes with fatty acid and their tribological properties as lubricant additive, Carbon 43 (2005) 1660–1665.
[26] J. Li, T. Tang, X. Zhang, S. Li, M. Li, Dissolution, characterization and photo-functionalization of carbon nanotubes, Mater. Lett. 61 (2007) 4351–4353.
[27] R. Wang, L. Shi, C.Y. Tang, S. Chou, C. Qiu, A.G. Fane, Characterization of novel forward osmosis hollow fiber membranes, J. Membr. Sci. 355 (2010) 158–167.
[28] H. Ma, C. Burger, B.S. Hsiao, B. Chu, Highly permeable polymer membranes containing directed channels for water purification, ACS Macro Lett. 1 (2012) 723–726.
[29] C.Y. Tang, Q. She, W.C.L. Lay, R. Wang, A.G. Fane, Coupled effects of internal concentration polarization and fouling on flux behavior of forward osmosis membranes during humic acid filtration, J. Membr. Sci. 354 (2010) 123–133.
[30] H.Y. Ng, W. Tang, W.S. Wong, Performance of forward (direct) osmosis process: Membrane structure and transport phenomenon, Environ. Sci. Technol. 40 (2006) 2408–2413.